Electron beam collimation with a 40 000 tip metallic double-gate field emitter array and in-situ control of nanotip sharpness distribution

Helfenstein, P ; Guzenko, V A ; Fink, H W ; Tsujino, S

Abstract: The generation of highly collimated electron beams from a double-gate field emitter array with 40000 metallic tips and large collimation gate apertures is reported. Field emission beam measurements demonstrated the reduction of the beam envelope down to the array size by applying a negative potential to the on-chip gate electrode for the collimation of individual field emission beamlets. Owing to the optimized gate structure, the concomitant decrease of the emission current was minimal, leading to a net enhancement of the current density. Furthermore, a noble gas conditioning process was successfully applied to the double-gate device to improve the beam uniformity in-situ with orders of magnitude increase of the active emission area. The results show that the proposed double-gate field emission cathodes are promising for high current and high brightness electron beam applications such as free-electron lasers and THz power devices.

DOI: https://doi.org/10.1063/1.4788998

Electron beam collimation with a 40000 tip metallic double-gate field emitter array and in-situ control of nanotip sharpness distribution

P. Helfenstein, V. A. Guzenko, H.-W. Fink, and S. Tsujino

Citation: Journal of Applied Physics **113**, 043306 (2013); doi: 10.1063/1.4788998
View online: http://dx.doi.org/10.1063/1.4788998
View Table of Contents: http://scitation.aip.org/content/aip/journal/jap/113/4?ver=pdfcov
Published by the AIP Publishing

Electron beam collimation with a 40 000 tip metallic double-gate field emitter array and in-situ control of nanotip sharpness distribution

P. Helfenstein,[1,a)] V. A. Guzenko,[1] H.-W. Fink,[2] and S. Tsujino[1,b)]
[1]*Laboratory for Micro- and Nanotechnology, Paul Scherrer Institut, CH-5232 Villigen-PSI, Switzerland*
[2]*Physik Institut, University of Zurich, Winterthurerstrasse 190, CH-8057 Zurich, Switzerland*

(Received 10 December 2012; accepted 7 January 2013; published online 24 January 2013)

The generation of highly collimated electron beams from a double-gate field emitter array with 40000 metallic tips and large collimation gate apertures is reported. Field emission beam measurements demonstrated the reduction of the beam envelope down to the array size by applying a negative potential to the on-chip gate electrode for the collimation of individual field emission beamlets. Owing to the optimized gate structure, the concomitant decrease of the emission current was minimal, leading to a net enhancement of the current density. Furthermore, a noble gas conditioning process was successfully applied to the double-gate device to improve the beam uniformity *in-situ* with orders of magnitude increase of the active emission area. The results show that the proposed double-gate field emission cathodes are promising for high current and high brightness electron beam applications such as free-electron lasers and THz power devices. © *2013 American Institute of Physics*. [http://dx.doi.org/10.1063/1.4788998]

I. INTRODUCTION

The extremely high brightness of field emission electron beams has enabled the realization of electron microscopes with single-atom resolution[1] and has stimulated high current and high current density applications such as free-electron lasers[2,3] and THz vacuum electronic devices.[4–7] Field emitters can produce high brightness electron beams via quantum tunneling by applying a strong electric field in the order of GV/m to solid surfaces. Such fields can be created by a comparatively low potential with the help of the field enhancement at the nanometer-scale tip apexes. The recognition that the electric field enhancement occurs not only at dc but also at high frequencies up to nearly optical frequencies has recently triggered intensive studies ranging from fundamental physics such as electron dynamics in strong fields[8] to ultrafast electron beam applications for time-resolved electron diffraction and microscopy,[9] potentially down to the attosecond range.[10]

Field emitter arrays (FEAs) with on-chip electron extraction gate electrodes G_{ext}, which combine the electron emission of thousands to millions of nanotips, have been explored for high current generation with a wide variety of materials.[7,11–14] To generate high brightness beams with a small transverse electron velocity spread, however, it is crucial to add an on-chip gate electrode G_{col} for the collimation of individual field emission beamlets. These so-called double-gate FEAs have been proposed as high current and high brightness cathodes[15,16] and have been actively studied.[17–26] One of the critical obstacles for the realization of high performance double-gate FEAs is the reduction of the emission current during the beam collimation. Recent developments show that this can be circumvented by devising the gate aperture shapes as demonstrated with volcano-shaped FEAs[23] and stacked double-gate device with large G_{col} apertures.[24–26]

For the practical application of FEAs it is important to prepare an array with uniform nanotip apex distribution. Due to the exponential sensitivity of the field emission current on the electric field at the emitter apexes, even a small non-uniformity of the emitter tip apex radius of curvature r_{tip} results in a highly non-uniform beam across the array and limits the total current, making the requirement for the r_{tip} uniformity stringent.[22] In the case of single-gate FEAs, the r_{tip} distribution of as-fabricated FEAs can be improved by an application of high potential switching pulses and blunting the emitter tips by joule heating[27] but at the expense of risking failure by vacuum arcs. Another promising method is the bombardment of ions generated by glow-discharge[28] or by electron impact ionization using the field emission current.[29–32] In particular, an improvement of the beam uniformity by *in-situ* noble gas conditioning for single-gate molybdenum FEAs was demonstrated recently.[32] However, no study has been reported for the beam uniformity control of double-gate FEAs.

In this work, we study the beam collimation characteristics and *in-situ* control of the r_{tip} distribution of a 40 000 tip double-gate FEAs with large G_{col} apertures. The experimental results demonstrated a substantial reduction of the transverse electron beam spread by G_{col} and an improvement of the beam uniformity by the noble-gas conditioning process.

II. EXPERIMENT & METHODS

A. Double-gate FEA fabrication

The double-gate FEA of pyramidal-shaped molybdenum nanotips with r_{tip} of ~10 nm, Figure 1, was fabricated by a combination of molding for the preparation of the emitter arrays, the self-aligned polymer etch-back method for the G_{ext} fabrication, and an electron beam (e-beam) lithography

[a)]Electronic mail: patrick.helfenstein@psi.ch.
[b)]Electronic mail: soichiro.tsujino@psi.ch.

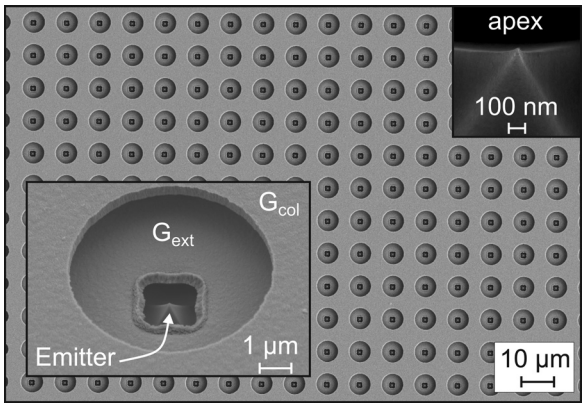

FIG. 1. SEM image of a part of the double-gate FEA with 4×10^4 molybdenum emitter tips. The insets show a close up of a single emitter with extraction (G_{ext}) and collimation gate (G_{col}) aperture openings (left bottom) and the tip-apex (right top).

process for the G_{col} fabrication.[25,26,33–35] The 4×10^4 emitter tips were aligned with 10 μm pitch in a circular area measuring 2.26 mm in diameter. The gate electrodes consisted of 0.5 μm thick molybdenum films. The FEA and G_{ext} were separated by a 1.2 μm thick SiO_2 layer, whereas G_{col} and G_{ext} were separated by a 1.2 μm thick SiON layer.[26] To pattern the apertures of G_{col}, a process using focused ion beam milling was formally developed for arrays up to 20×20 tips.[25,26] This maskless and flexible method is ideal for prototyping small arrays but difficult to apply to larger FEAs because of the required milling time of ~90 s per aperture. With the newly developed e-beam process, we successfully prepared the 4×10^4 tip FEA having a G_{col} aperture diameter of 6.5 ± 0.1 μm, which is a factor of 3 larger than that of the G_{ext} apertures (2.0 ± 0.1 μm).[35] Patterning the gate apertures with this ratio was difficult with the polymer-etch back method but critically important to achieve a high current density enhancement with a small transverse electron velocity spread.[24–26]

B. Field emission experiment

The experiment was conducted in a field emission microscope, Figure 2, equipped with an electron beam imaging screen (metalized P43 phosphor) and a retractable Faraday cup. The FEA was placed 50 mm from the screen. A CCD camera was used to record the beam images which were subsequently analyzed to evaluate the rms beam radius R_s and the rms transverse velocity u_t.[26] We simultaneously measured the current I_{em} through the FEA and the gate currents I_{ext} and I_{col}, Figure 2. The net current I_{net} reaching the screen was evaluated from the relation ($|I_{em}| - I_{ext} - I_{col}$). The field emission beam was accelerated by a potential of 3 kV applied to the screen. Alternatively, I_{net} was measured directly by the Faraday cup biased at 300–500 V. The value of I_{net} was the same for the two measurements.

In the beam collimation experiment, we simultaneously varied V_{col} and V_{em} with a fixed ratio k_{col} ($=V_{col}/V_{em}$) and recorded the beam images at the largest V_{em}. The beam was measured at different collimation strengths by scanning k_{col} from 0 to 0.9 in steps of 0.1 and from 0.91 to 1.05 in steps

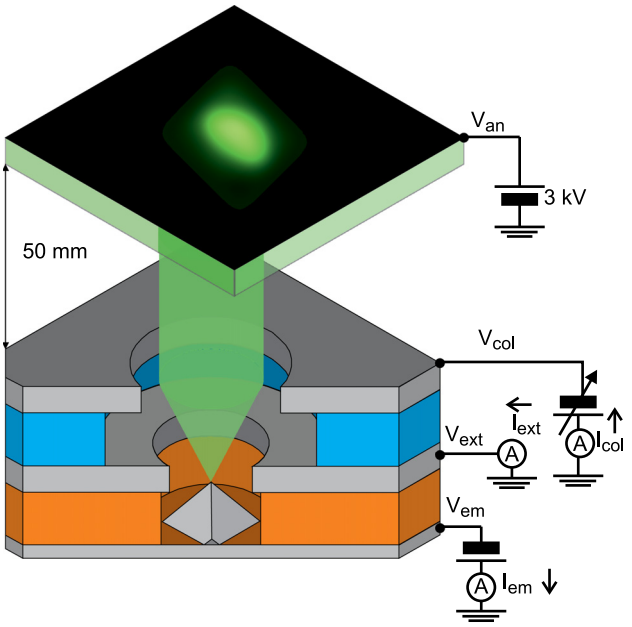

FIG. 2. Schematic illustration of the experimental setup. The double-gate FEA in the field emission microscope generates a collimated electron beam under the potential voltages V_{em}, V_{ext}, and V_{col}. The currents I_{em}, I_{ext}, and I_{col} were simultaneously monitored to evaluate the current I_{net} reaching the screen. Using a retractable Faraday cup (not shown), I_{net} can be measured directly.

of 0.01. To restrict the power consumption of the screen, we limited the maximum I_{net} to ~5 μA.

After inserting the FEA into the field emission microscope, the chamber was evacuated to the base pressure of $\sim 5 \times 10^{-9}$ mbar. Then, the FEA was conditioned by scanning the potential V_{em} applied to the emitter substrate between 0 V and a negative maximum for several days until the emission current level became stable.[26] During this conditioning phase, the gate potentials V_{ext} and V_{col} were set to ground potential. We further conditioned the FEA in a low-pressure Ne gas atmosphere by continuing the V_{em} scan for ~3 h after introducing neon gas at a pressure of $(1–2) \times 10^{-4}$ mbar into the chamber. The relation between the Faraday cup current and V_{em} was continuously recorded and analyzed.

C. Theoretical modeling of the double-gate FEAs

To analyze the experiment, we created a 3D model of a single emitter using commercial tools: CST Particle Studio for the particle tracking simulation and COMSOL Multiphysics for calculating the static electric field at the emitter tip surface. We assumed an r_{tip} of 10 nm and applied the Fowler-Nordheim equation at the emitter surface to calculate the emission current distribution.[36] By subsequently integrating the equation of motion for electrons emitted from the nanotip surfaces, the beam collimation characteristics under the influence of the gate potential field were calculated.

III. EXPERIMENTAL RESULTS

A. Electron beam characteristics

Figures 3–5 show the observed electron beam characteristics of the double-gate FEA. The beam images of Figures

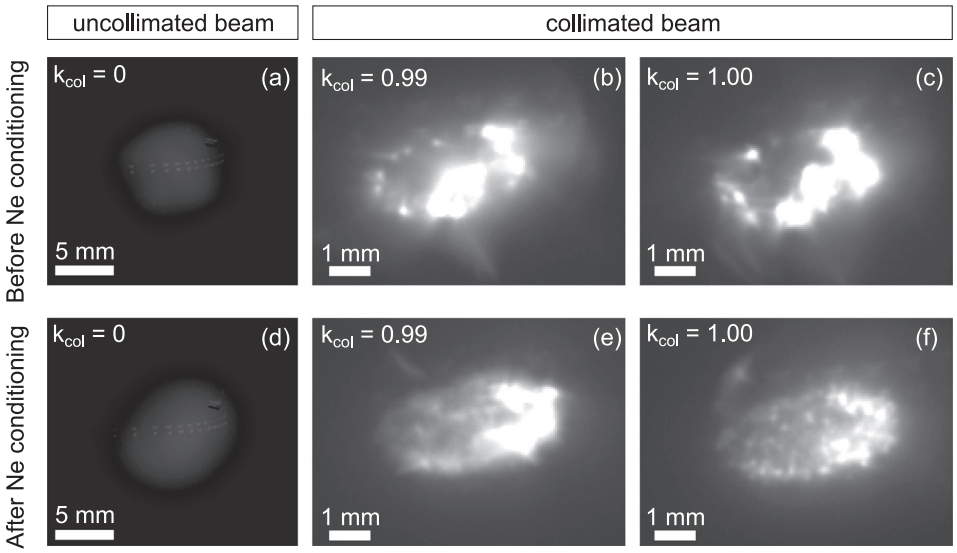

FIG. 3. Images of field emission beams generated by the double-gate FEA with 4×10^4 emitters at different collimation strength denoted by the ratio k_{col} ($=V_{col}/V_{em}$). (a)-(c) were observed before the Ne gas conditioning with V_{em} of -72 V, whereas (d)-(f) were observed after the Ne gas conditioning with V_{em} of -69 V. The maximum current reaching the screen at zero k_{col} was $\sim 5\,\mu$A for both cases. All the beams are displayed with the same intensity scale, highlighting the large beam brightness enhancement at k_{col} of 0.99 and 1.00.

3(a)–3(c) show that the increase of k_{col} from 0 to 0.99 and 1.00 enhanced the beam brightness considerably. Owing to the large G_{col} apertures, more than 30% of the current emitted from the tips was retained at the maximum collimation.[26] This resulted in an enhanced current density with the decrease of $R_s - R_0$, where R_0 equal to 0.57 mm is the rms radius of the FEA. In fact, the I-V characteristics in Figures 5(a) and 5(b) and the variation of $R_s - R_0$ in Figure 4 (open squares) show that increasing k_{col} from 0 to 0.99 resulted in a decrease of I_{net} from $5.5 \pm 0.2\,\mu$A to $1.9 \pm 0.2\,\mu$A, whereas $R_s - R_0$ decreased from 2.9 ± 0.2 mm to 0.1 ± 0.1 mm. Since the beam area decreased more rapidly than I_{net}, this resulted in an enhanced beam brightness. The similarity of this result to the previously reported experiments with FEAs with a smaller number of tips[25,26] demonstrates the capability to upscale the excellent beam characteristics of 4-400 emitters up to 4×10^4 emitters.

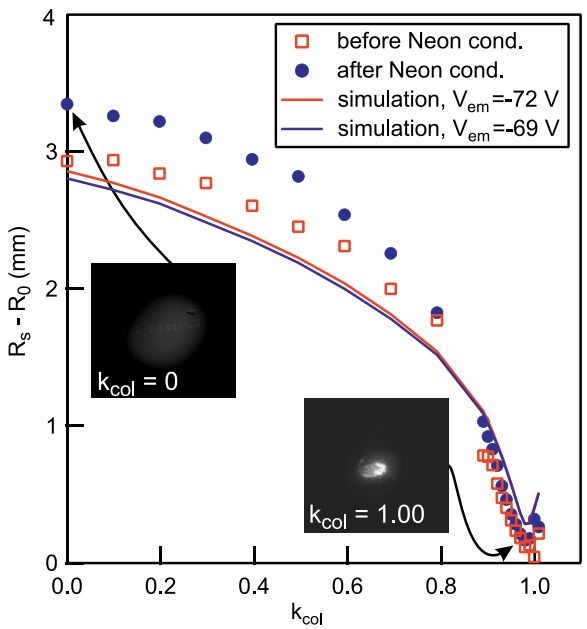

FIG. 4. Variation of R_s with the increase of k_{col} before and after the neon conditioning. The rms radius R_0 equal to 0.57 mm of the FEA was subtracted from R_s for the experiment. The solid lines show the calculated R_s versus k_{col} obtained by the full 3D simulation of a single-emitter at values of V_{em} equal to -72 V and -69 V. The beam images at k_{col} equal to 0 and 1.00 at V_{em} of -69 V obtained after the neon gas conditioning are also displayed.

The beneficial effect of the large G_{col} apertures was also supported by theory. From the single emitter simulation, we calculated the beam characteristics for k_{col} between 0 and 1.05. The simulated I-V characteristics at V_{em} of -72 V and -69 V calculated simultaneously with the beam characteristics are shown in Figures 5(c) and 5(d), respectively. The calculated beam collimation characteristics of the single emitter are shown in Figure 4 for the two V_{em} values (solid lines). (We note that the rms source radius of the single emitter ($\ll$10 nm) is negligible in this scale). The reproduction of the experimental values of the shape of the I-V variation and the beam collimation characteristics as functions of k_{col} are excellent.

The comparison of Figures 3(b) and 3(c) with Figures 3(e) and 3(f) shows that the neon gas conditioning improved the beam uniformity. At approximately the same I_{net} with a slightly smaller V_{em} of -69 V, the beam observed after the gas conditioning exhibited fewer parts with nearly saturated intensity and increased emission around the center of the beam, whereas the $R_s - R_0$ versus k_{col} relation was approximately the same. The I-V characteristics (Figure 5(a)) changed slightly after the neon conditioning (Figure 5(b)). Interestingly, the shape of the I-V characteristics after the gas conditioning (Figure 5(b)) resembles that of simulation more closely. One can ascribe this as a consequence of making the r_{tip} distribution more uniform by the neon gas conditioning. The same shape of the two calculated I-V curves at V_{em} of -72 V and -69 V (Figures 5(c) and 5(d), respectively) shows that the difference of V_{em} in the two experiments is not the source of the different curve shapes.

To quantify the quality of the collimated electron beam, we evaluated the rms transverse velocity u_t evaluated by the following equation[26]

$$\frac{R_s - R_0}{L_s} \approx \frac{2u_t}{u_{an}} \left(\sqrt{1 + \frac{u_0^2}{u_{an}^2}} - \frac{u_0}{u_{an}} \right). \quad (1)$$

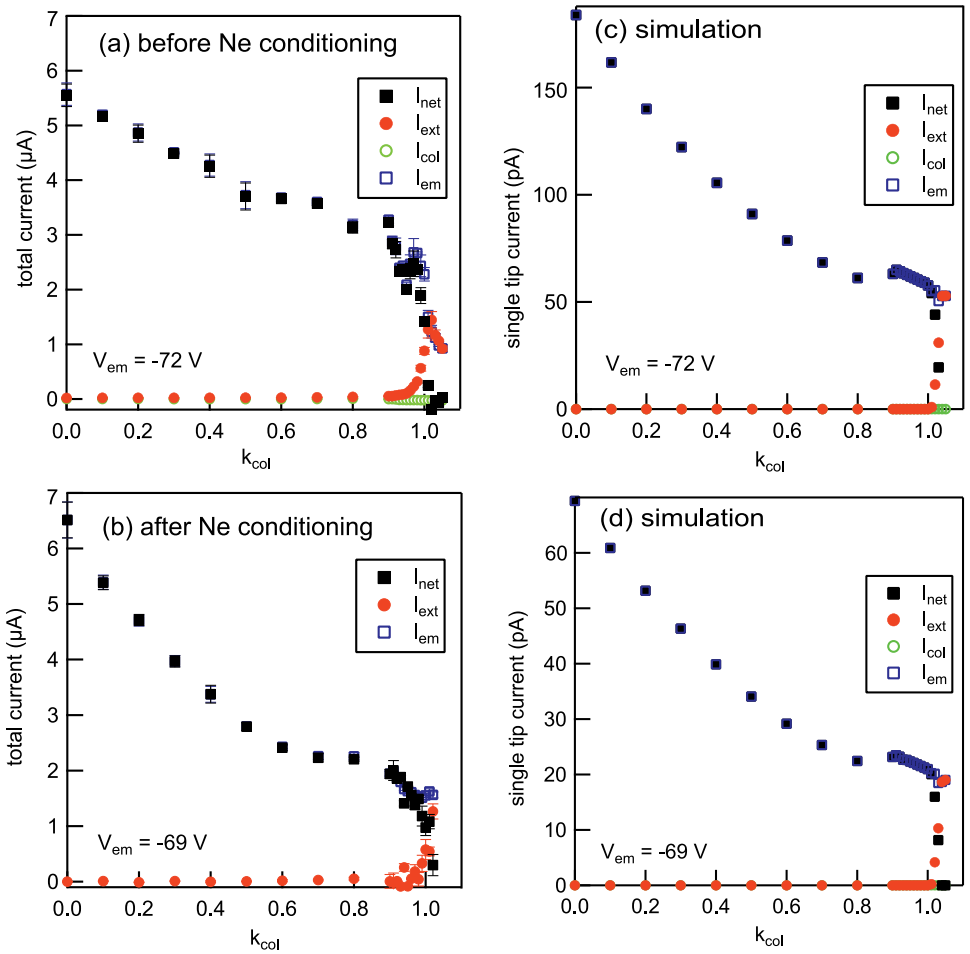

FIG. 5. Current-voltage characteristics of the 40 000 tip FEA measured during the beam collimation experiment of Figure 3, (a) before the neon gas conditioning with V_{em} of −72 V, (b) after the neon gas conditioning with V_{em} of −69 V. The simulated current-voltage characteristics (c) at V_{em} of −72 V and (d) at V_{em} of −69 V were obtained together with the calculation of the $R_s - k_{col}$ relations displayed in Figure 4.

In above equation, L_s of 50 mm is the distance between the FEA and the screen, and u_{an} is the longitudinal velocity at the screen determined by V_{an} of 3 kV as $\sqrt{2q|V_{an}|/m}$ (q being the elementary charge and m is the electron rest mass). u_0 is the initial longitudinal velocity defined at a few microns off the tip surface. At $k_{col} = 0$, it is approximately given by $\sqrt{2q|V_{em}|/m}$. At k_{col} close to unity, u_0 can be safely neglected because the electrons are significantly decelerated by V_{col}. Since V_{an} is an order of magnitude larger than V_{col}, we neglected the effect of V_{col}.

At zero k_{col}, from $R_s - R_0$ of 2.9 ± 0.2 mm and Eq. (1), u_t as a fraction of the speed of light in vacuum c_0 is evaluated to be $(3.7 \pm 0.1) \times 10^{-3}$. At $k_{col} = 0.99$ with $R_s - R_0$ equal to 0.16 ± 0.1 mm, u_t/c_0 is evaluated to be $\sim 2.4 \times 10^{-4}$. The reduction of u_t by a factor of ~15 is about 1.5 times better than the previous results obtained from FEAs with a smaller number of emitters.[25,26]

We note that a close inspection of the beam images at k_{col} of 0.99 and 1.00 in Figure 3, in particular Figures 3(e) and 3(f), reveals granular spots with a typical rms radius below ~100 μm. This value is approaching the experimental resolution and is in the same order of magnitude as the calculated single emitter value. The similarity of these images with the granular beam images of as-fabricated single-gate FEAs observed at the acceleration potential of 200 kV using a pulsed diode gun[32,37,38] poses a possibility that individual beamlets were resolved at the large k_{col} values in the present experiment, even though the acceleration potential was only 3 kV and there was no additional focusing element such as a solenoid. This suggests that the actual minimal value of u_t is smaller than the value evaluated above from the beam envelope. Further experiments concerning the direct measurement of the transverse beam emittance and analysis of the model at high k_{col} as a function of high acceleration fields are needed to establish the actual collimation strength.

B. Emission homogenization by noble gas conditioning

Finally, we discuss the impact of the neon gas conditioning on the emission characteristics. Figure 6(a) shows the evolution of the relation between I_{net} and V_{em} during the conditioning. As a result of ~3 h of the neon gas conditioning, the current at a given V_{em} increased approximately an order of magnitude (from scan a to scan c), with I_{net} reaching 0.14 mA at a V_{em} of −81 V in the end.

We analyzed the I_{net}-V_{em} relation by fitting with the following function

$$I = A_{FN}\left(\frac{|V_{em}|}{B_{FN}}\right)^2 \exp\left(\frac{-B_{FN}}{|V_{em}|}\right). \quad (2)$$

This assumes the Fowler-Nordheim equation for the single-tip current I_{tip} with a constant single-tip emission area S_{tip}

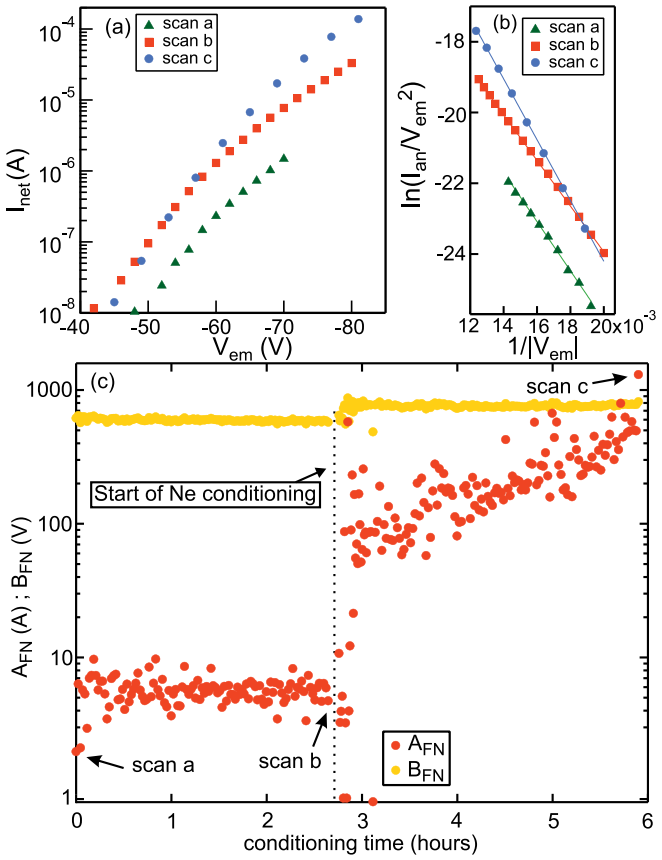

FIG. 6. (a) Evolution of the emission current-voltage characteristics during the conditioning. (b) Fowler-Nordheim plot of the I-Vs shown in (a). (c) The evolution of the Fowler-Nordheim fitting parameters A_{FN} and B_{FN} in UHV and during the neon gas conditioning.

and an electric field F at the emitter tip apex determined by $|V_{em}|$[36,39–41]

$$I_{tip} = S_{tip}\frac{a}{t^2\phi}\exp(bc^2/\sqrt{\phi})F^2\exp\left(-\frac{b\phi^{3/2}}{F}\right), \quad (3)$$

where S_{tip} is the single-tip emission area and F is the electric field at the emitter tip apex. The constants a, b, c are given by $a = 1.541434 \times 10^{-6}$ A eV V^{-2}, $b = 6.830890$ eV$^{-3/2}$ Vnm^{-1}, and $c = 1.199985$ eV V$^{-1/2}$ nm$^{1/2}$. ϕ is the work function (~4.5 eV for molybdenum), and t is approximately equal to 1.[36,42] The fitting parameters A_{FN} and B_{FN} are written as follows

$$A_{FN} = N_{tip}S_{tip}\frac{ab^2\phi^2}{t^2}\exp(bc^2/\sqrt{\phi}), \quad (4)$$

$$B_{FN} = b\phi^{3/2}\beta^{-1}, \quad (5)$$

where N_{tip} is the number of active emitters and β is the field enhancement factor (equal to $F/|V_{em}|$). β is approximately proportional to $(r_{tip})^{-0.5}$ for our pyramidal shaped emitters.[43]

Figure 6(c) summarizes the obtained evolution of A_{FN} and B_{FN}. At the end of the conditioning in UHV and before the neon gas was introduced in the chamber, A_{FN} was equal to 5±2 A and B_{FN} was equal to ~650 V. When the neon gas was introduced into the chamber, B_{FN} increased to ~840 V during the first 10 min and remained approximately unchanged. After the conditioning, A_{FN} increased to ~10^3 A. Referring to Eq. (5), the 30% increase of B_{FN} at the beginning of the neon gas conditioning is ascribed to the increase of ϕ or the decrease of β via an increase of r_{tip}. The decreased fraction of extremely bright spots after the conditioning indicates that the conditioning blunted the sharpest emitters that were already active before, suggesting the increase of r_{tip}. Since A_{FN} decreases with the increase of ϕ (see Eq. (4)), the observed increase of A_{FN} by two orders of magnitude suggests that N_{tip} increased by the same orders of magnitude. These conclusions are compatible with the observed beam uniformity improvement, Figure 3.

The observed effect of the neon conditioning is different from previously reported experiments. In the glow-discharge processing of Spindt single-gate FEAs,[28] the bombardment of neon and hydrogen ions generated by glow-discharge on the FEA decreased B_{FN} but only a small change in A_{FN} resulted. The well-known finishing procedure of etched-wire needle-shape field emitters[44–46] is similar to our method in appearance but different in effect: the irradiation of the neon gas ions created by the impact ionization of the field emitted electrons to the emitter tip results in sharpening of the tip down to a few atoms. In contrast, our observation indicates that the neon gas had blunted the sharp tips while at the same time activating non-emitting tips. We note that the previous report on the noble-gas conditioning of single-gate FEAs for longer time periods increased B_{FN} by more than a factor of 2 together with orders of magnitude increase of A_{FN}. The nature of these different consequences under the different plasma conditions have not been elucidated yet. Since the gas processing is a promising method to improve the beam uniformity and the maximum current, further investigation on the precise physical origin of the observed effect is an urgent task and the subject of intense research.

IV. CONCLUSIONS

In summary, we showed the successful fabrication of a double-gate FEA with 4×10^4 tips with large G_{col} apertures using e-beam lithography and demonstrated its excellent electron beam collimation characteristics. By submitting the FEA to a low pressure neon gas, we were able to increase the active emission area and to obtain a more homogeneous beam. The successful reproduction of the experiment by a full 3D simulation of a single emitter for the beam collimation characteristics and the emission current characteristics was also shown and demonstrates that it is feasible to use the established model for further optimization of the gate structure and to study the beam emission and collimation characteristics under high acceleration electric field.

The collimation of the beam envelope down to the FEA diameter and the hint of resolving individual emitters at low (3 keV) acceleration potential show that the rms transverse velocity was reduced to a significantly low value. To establish this fact with increased resolution on the beam diagnostics, further investigations including the direct beam

emittance measurement using the DC gun test-stand[47,48] and experiments with single-emitters are under way.

ACKNOWLEDGMENTS

The authors acknowledge J. Leemann, K. Vogelsang, and A. Luecke for their help for the FEA fabrication. This work was conducted within the SwissFEL project at the Paul Scherrer Institute and was partially supported by the Swiss National Science Foundation No. 200021_125084.

[1]A. V. Crewe, J. Wall, and J. Langmore, Science **168**, 1338 (1970).
[2]C. Brau, Nucl. Instrum. Methods Phys. Res. **407**, 1 (1998).
[3]B. D. Patterson, R. Abela, H. H. Braun, U. Flechsig, R. Ganter, Y. Kim, E. Kirk, A. Oppelt, M. Pedrozzi, S. Reiche, L. Rivkin, T. Schmidt, B. Schmitt, V. N. Strocov, S. Tsujino, and A. F. Wrulich, New J. Phys. **12**, 035012 (2010).
[4]H. Makishima, S. Miyano, H. Imura, J. Matsuoka, H. Takemura, and A. Okamoto, Appl. Surf. Sci. **146**, 230 (1999).
[5]D. Whaley, R. Duggal, C. Armstrong, C. Bellew, C. Holland, and C. Spindt, IEEE Trans. Electron Devices **56**, 896 (2009).
[6]J. H. Booske, Phys. Plasmas **15**, 055502 (2008).
[7]K. B. K. Teo, E. Minoux, L. Hudanski, F. Peauger, J.-P. Schnell, L. Gangloff, P. Legagneux, D. Dieumegard, G. A. J. Amaratunga, and W. I. Milne, Nature **437**, 968 (2005).
[8]G. Herink, D. R. Solli, M. Gulde, and C. Ropers, Nature **483**, 190 (2012).
[9]A. H. Zewail, Annu. Rev. Phys. Chem. **57**, 65 (2006).
[10]M. Kruger, M. Schenk, and P. Hommelhoff, Nature **475**, 78 (2011).
[11]C. A. Spindt, I. Brodie, L. Humphrey, and E. R. Westerberg, J. Appl. Phys. **47**, 5248 (1976).
[12]P. R. Schwoebel, C. A. Spindt, and C. E. Holland, J. Vac. Sci. Technol. B **23**, 691 (2005).
[13]R. C. Smith and S. R. P. Silva, Appl. Phys. Lett. **94**, 133104 (2009).
[14]C. Li, Y. Zhang, M. T. Cole, S. G. Shivareddy, J. S. Barnard, W. Lei, B. Wang, D. Pribat, G. A. J. Amaratunga, and W. I. Milne, ACS Nano **6**, 3236 (2012).
[15]C. M. Tang, A. C. Ting, and T. Swyden, Nucl. Instrum. Methods Phys. Res. **318**, 353 (1992).
[16]M. Dehler, A. Candel, and E. Gjonaj, J. Vac. Sci. Technol. B **24**, 892 (2006).
[17]J. Itoh, Y. Toma, K. Morikawa, S. Kanemaru, and K. Shimizu, J. Vac. Sci. Technol. B **13**, 1968 (1995).
[18]Y. Yamaoka, S. Kanemaru, and J. Itoh, Jpn. J. Appl. Phys. **35**, 6626 (1996).
[19]C. Py, J. Itoh, T. Hirano, and S. Kanemaru, IEEE Trans. Electron Devices **44**, 498 (1997).
[20]A. Hosono, S. Kawabuchi, S. Horibata, S. Okuda, H. Harada, and M. Takai, J. Vac. Sci. Technol. B **17**, 575 (1999).
[21]C. Py, M. Gao, S. R. Das, P. Grant, P. Marshall, and L. LeBrun, J. Vac. Sci. Technol. A **18**, 626 (2000).
[22]L. Dvorson, G. Sha, I. Kymissis, C. Y. Hong, and A. I. Akinwande, IEEE Trans. Electron Devices **50**, 2548 (2003).
[23]Y. Neo, M. Takeda, T. Soda, M. Nagao, T. Yoshida, S. Kanemaru, T. Sakai, K. Hagiwara, N. Saito, T. Aoki, and H. Mimura, J. Vac. Sci. Technol. B **27**, 701 (2009).
[24]S. Tsujino, P. Helfenstein, E. Kirk, T. Vogel, C. Escher, and H.-W. Fink, IEEE Electron Device Lett. **31**, 1059 (2010).
[25]P. Helfenstein, E. Kirk, K. Jefimovs, T. Vogel, C. Escher, H.-W. Fink, and S. Tsujino, Appl. Phys. Lett. **98**, 061502 (2011).
[26]P. Helfenstein, K. Jefimovs, E. Kirk, T. Vogel, C. Escher, H.-W. Fink, and S. Tsujino, J. Appl. Phys. **112**, 093307 (2012).
[27]P. R. Schwoebel, C. A. Spindt, C. E. Holland, and J. A. Panitz, J. Vac. Sci. Technol. B **19**, 980 (2001).
[28]P. R. Schwoebel and C. A. Spindt, J. Vac. Sci. Technol. B **12**, 2414 (1994).
[29]I. Brodie, Int. J. Electron. **38**, 541 (1975).
[30]C. M. Marrese, "Compatibility of field emission cathode and electric propulsion technologies," Ph.D. thesis (University of Michigan, 1999).
[31]D. Nicolaescu, M. Nagao, T. Sato, V. Filip, S. Kanemaru, and J. Itoh, J. Vac. Sci. Technol. B **23**, 707 (2005).
[32]S. Tsujino, M. Paraliev, E. Kirk, and H.-H. Braun, Appl. Phys. Lett. **99**, 073101 (2011).
[33]E. Kirk, S. Tsujino, T. Vogel, K. Jefimovs, J. Gobrecht, and A. Wrulich, J. Vac. Sci. Technol. B **27**, 1813 (2009).
[34]A. Mustonen, P. Beaud, E. Kirk, T. Feurer, and S. Tsujino, Appl. Phys. Lett. **99**, 103504 (2011).
[35]V. A. Guzenko, A. Mustonen, P. Helfenstein, E. Kirk, and S. Tsujino, Microelectron. Eng. (submitted).
[36]R. G. Forbes and J. H. Deane, Proc. R. Soc. London, Ser. A **463**, 2907 (2007).
[37]S. Tsujino, M. Paraliev, E. Kirk, T. Vogel, F. L. Pimpec, C. Gough, S. Ivkovic, and H.-H. Braun, J. Vac. Sci. Technol. B **29**, 02B117 (2011).
[38]S. Tsujino, M. Paraliev, E. Kirk, C. Gough, S. Ivkovic, and H.-H. Braun, Phys. Plasmas **18**, 064502 (2011).
[39]J. M. Houston, Phys. Rev. **88**, 349 (1952).
[40]R. E. Burgess, H. Kroemer, and J. M. Houston, Phys. Rev. **90**, 515 (1953).
[41]R. G. Forbes, J. Vac. Sci. Technol. B **17**, 526 (1999).
[42]F. R. Abbott and J. E. Henderson, Phys. Rev. **56**, 113 (1939).
[43]S. Tsujino, F. le Pimpec, J. Raabe, M. Buess, M. Dehler, E. Kirk, J. Gobrecht, and A. Wrulich, Appl. Phys. Lett. **94**, 093508 (2009).
[44]A. P. Janssen and J. P. Jones, J. Phys. D **4**, 118 (1971).
[45]R. Smith, J. Phys. D **17**, 1045 (1984).
[46]S. Ernst, S. Wirth, M. Rams, V. Dolocan, and F. Steglich, Sci. Technol. Adv. Mater. **8**, 347 (2007).
[47]S. C. Leemann, A. Streun, and A. F. Wrulich, Phys. Rev. ST Accel. Beams **10**, 071302 (2007).
[48]S. Tsujino, M. Paraliev, P. Helfenstein, and H.-H. Braun, in *Vacuum Nanoelectronics Conference (IVNC), 25th International*, 2012, pp. 1–2.